




Review

Review on Floating Offshore Wind Turbine Models for Nonlinear Control Design

Hedi Basbas ¹, Yong-Chao Liu ¹, Salah Laghrouche ¹, Mickaël Hilaiet ^{1,*} and Franck Plestan ²

¹ FEMTO-ST Institute, Université Bourgogne Franche-Comté, UTBM, CNRS Rue Ernest Thierry Mieg, F-90000 Belfort, France; hedi.basbas@utbm.fr (H.B.); yongchao.liu@utbm.fr (Y.-C.L.); salah.laghrouche@utbm.fr (S.L.)

² Ecole Centrale Nantes, CNRS, LS2N, UMR 6004, Nantes Université, F-44000 Nantes, France; franck.plestan@ec-nantes.fr

* Correspondence: mickael.hilaiet@univ-fcomte.fr

Abstract: This article proposes a review of the modeling approaches for floating offshore wind turbines (FOWTs) for nonlinear control design. The aerodynamic, hydrodynamic and mooring line dynamic modules for the FOWT have been reviewed to provide an overview of several modeling approaches with their respective features. Next, three control-oriented models from the literature are revisited by presenting their methodological approaches to modeling and identification. These three models cover the three most popular types of FOWTs. Then, the performances of these models are validated with the open fatigue, aerodynamics, structures, and turbulence (OpenFAST) code, and their performances are evaluated according to several criteria. Finally, one of the three models is used to illustrate a nonlinear second-order sliding mode control based on the twisting algorithm to optimize the performance of the FOWT in terms of energy extraction and reduction in the platform pitch oscillation.

Keywords: floating offshore wind turbine; control-oriented models; model-based control



Citation: Basbas, H.; Liu, Y.-C.; Laghrouche, S.; Hilaiet, M.; Plestan, F. Review on Floating Offshore Wind Turbine Models for Nonlinear Control Design. *Energies* **2022**, *15*, 5477. <https://doi.org/10.3390/en15155477>

Academic Editors: Thierry A. Meynard and Jaime W. Zapata

Received: 27 June 2022

Accepted: 19 July 2022

Published: 28 July 2022

Publisher's Note: MDPI stays neutral with regard to jurisdictional claims in published maps and institutional affiliations.



Copyright: © 2022 by the authors. Licensee MDPI, Basel, Switzerland. This article is an open access article distributed under the terms and conditions of the Creative Commons Attribution (CC BY) license (<https://creativecommons.org/licenses/by/4.0/>).

1. Introduction

The harvesting of wind energy using onshore wind turbines is a mature control system. Recently, offshore wind turbines have been developed off the coast, with several wind farms in operation that offer higher-power outputs than onshore wind farms. Because 80% of wind resources in marine environments are found in deep waters (greater than 60 m deep) [1], installing wind turbines in these areas would help the production of renewable energy from wind with multiple advantages. Higher wind intensity could be expected with drastically better quality than inland. Furthermore, the visual and noise pollution would be pushed far from the coast, which represents one more advantage of floating offshore wind turbines (FOWTs). However, fixing the wind turbine to the seabed is no longer possible in deep waters due to financial and logistical constraints, hence the idea of mounting the turbines on floating platforms. **There are three popular types of FOWTs: the tensioned leg platform (TLP)-based FOWT, the spar-buoy FOWT and the semi-submerged FOWT (Figure 1).** Each of them presents different features depending on the financial, logistical and stability criteria [2]. However, compared with the fixed wind turbines, the complexity of the FOWT is significantly higher in terms of modeling for control design and the stability of the floating platform [3].

FOWTs are multi-physics systems mixing aerodynamics, hydrodynamics, mooring line dynamics and electrical machines associated with power converters and controllers. To enable the emergence of FOWTs, several models have been proposed in recent years. A classification can be proposed by separating the models highly faithful to reality and the reduced models. The first ones are models using precise calculation methods but they are often very heavy in resolution time. We can quote, for example, OpenFOAM, Ansys

AQWA, Autodesk, and ABAQUS, which use computational fluid dynamics (CFD) or the finite element method (FEM) to solve the equations. These two methods of resolution allow the detailed analysis of the phenomena and local loads applied at different points of the whole structure. One of the disadvantages of such solvers is that they are often commercial and are not available in open-source. Furthermore, for validation purposes of control laws or for the first development of the structure design, these programs require a considerable amount of computing time. Thus, other precise software allow for reduced calculation times such as open fatigue, aerodynamics, structures, and turbulence (OpenFAST), SimPack, HAWC2 for the complete modeling of the FOWT and Bladed Orcaflex for aerodynamic and hydrodynamic modeling, respectively. Computation times are reduced by combining highly accurate numerical methods (e.g., CFD) with less intensive computing ones. For preliminary structural designs or the development of innovative control laws, reduced models seem to be a better alternative. They are reduced to the most important dynamics, allowing a decrease in the computation resolution time. They describe the most important dynamics, allowing a reduction in the computation time and the design of the controls. The first ones are often linear models considering all the structures rigid. They allow the development of linear control laws around operating points. However, they cannot give transient analysis in the case of an irregular wave profile. **The second is nonlinear models [4–13], often used for the development of advanced nonlinear control laws. As FOWTs are highly nonlinear systems and subject to time-varying parameters, nonlinear time-domain models seem to be a suitable solution. These types of models are called Control-Oriented Models (COMs) in this study.** Based on it, multiple controllers have been proposed for the regulation of the rotor speed of the turbine and the attenuation of the pitch angle of the platform.

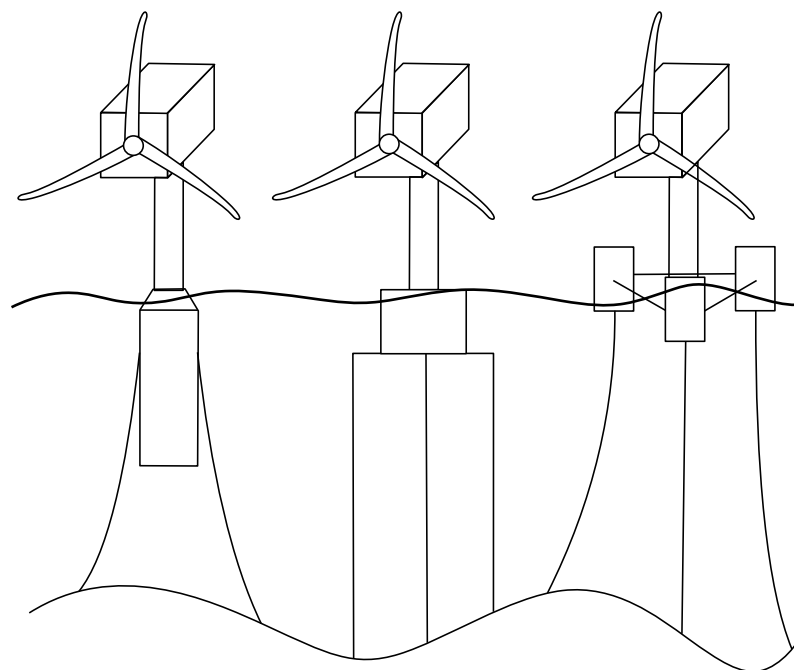


Figure 1. From left to right: Spar-buoy FOWT, TLP-based FOWT and semi-submerged FOWT.

The existing controllers designed for the FOWTs can be divided into two categories: one is the linear controller, and the other is the nonlinear controller. For the linear controller, classic proportional integral derivative (PID) controllers were used in floating wind turbines for the first time in the form of programmed gains [3,14,15]. It is important to note that the gain sizing task is performed offline and has the disadvantage of having to scale a multitude of gains. In [16], the individual blade pitch angle control of each blade has been generated by two expert PI controllers associated with a classic PI controller for the collective blade pitch angle control. Such strategy allows the intelligent adaptation of the gains by the experience

of the FOWT. In [17], a similar controller has been developed based on two coupled PID correctors for collective and individual blade pitch angle controls. The gains are defined online by the optimization of an objective function. However, such an optimization is computationally expensive and would be difficult in practice. Linear quadratic regulator (LQR) controllers have been proposed in [18,19]. The results have shown an improvement both in the rotor speed regulation and in the movement attenuation of the floating structure. However, linear controllers are not robust to parameter uncertainties, unmodeled dynamics or external perturbations. A nonlinear model predictive control (NMPC) strategy has been designed for Region 3 of the FOWT [20]. This control strategy uses a nonlinear prediction model to perform online optimization to compute the desired blade pitch angle control signal in each sampling period. The optimization process has not been validated in real-time due to the computational burden for such controllers. In [21], a switching linear parameter-varying (SLPV) control strategy based on linearized models of the FOWT has been proposed. In this strategy, the COM of the FOWT is linearized around several operating points to generate different linearized models of the FOWT, and then these models are used to optimize an objective function.

One of the most robust nonlinear controls is the sliding mode controller (SMC). This nonlinear strategy has been widely used in many areas [22–26] due to its attractive features, including robustness against disturbances and model uncertainties. The SMC can be divided into the first-order SMC and the high-order SMC (HOSMC). For the first-order SMC, the idea is to produce a discontinuous control signal to ensure that the state trajectory converges in finite time. Once this reaching phase is completed, these controllers ensure the robustness by keeping the state on the sliding manifold in the presence of perturbations and uncertainties. However, discontinuous signals could affect the real system through the so-called chattering. Thus n-HOSMC are applied to produce discontinuous signals in the n -derivative of the states such that the control signal is continuous as in [22,27]. Recently, Refs. [28,29] resumed the investigations of HOSMCs for FOWTs with the use of an adaptive model-free twisting algorithm. These papers have shown that these HOSMCs drastically reduce the tuning process time with fewer parameters than linear controllers. However, these SMCs are developed based on the linearized models from OpenFAST, which does not integrate all the nonlinear dynamics of the FOWT.

The main contributions of this article can be summarized as follows:

- A review of the general modeling approaches for the floating offshore wind turbine system.
- The focus is on the nonlinear COMs of FOWTs. Three of the best-known COMs have been selected and briefly reviewed to provide two comparative analyses based on the mathematical formulations of models and the simulation results.
- To emphasize the benefits of the nonlinear COMs for the development of nonlinear control laws, the model-based twisting algorithm is designed based on a selected nonlinear COM for the regulation of the rotor speed to its nominal value and for the attenuation of the oscillations of the platform pitch angle.

The rest of the article is organized as follows. In Section 2, a review of the different modeling approaches for the FOWT is presented. In Section 3, three existing COMs are reviewed and compared. Section 4 shows an application example where a model-based twisting sliding mode controller is designed for the regulation of the rotor speed at its reference value and for the attenuation of the platform pitch oscillations. Finally, the conclusion and the perspectives are given in Section 5.

2. Modeling Approach of FOWT

In this section, the different methodologies to model the FOWT are covered. Generally, complete wind turbine models consist of three main simulation blocks: (1) the mechanical structure made up of the float-tower-nacelle assembly, (2) the rotating wind turbine and (3) the generator model. The first block outputs the translational and rotational displacement states of the FOWT. This is achieved by using equations of motion based on the

fundamental mechanical formalisms presented in Section 2.1. The wind turbine model links the rotating blade shaft to the generator shaft with the drivetrain shaft equations presented in Section 2.5. The generator model is not retained here because the models are known and mature in the literature [30]. As depicted in Figure 2, the mechanical structure model links the state displacements to the external applied forces from aerodynamic, hydrodynamic and catenary line modules. This section reviews the motion equations with their derivations based on Newton–Euler and Lagrange formalism. Then, the aerodynamic, hydrodynamic, mooring line and drivetrain models for FOWTs are reviewed, followed by the wind and wave profile types. This section gives a general overview of the different modeling blocks and concepts of the FOWT models.

2.1. Equations of Motion

In mechanics, the equations of motion (EOM) give the translational and rotational displacements of a mechanical system depending on its environment (forces, energies, constraints, etc.). For the formulation of the EOM, the Newton–Euler formalism was initially proposed to express the body accelerations from the applied and constraint forces and moments. Several years later, the Newton–Euler formalism was followed by the Lagrange formalism, which gives the velocity displacements of a mechanical system in function of the potential and kinetic energies. Finally, Hamilton’s formalism continued Lagrange’s work with the concept of “least action”, which minimizes the integral action defined as the integral of the Lagrange operator between two points. The Newton–Euler formulation is generally used in Cartesian coordinates to express the EOM intuitively when all the forces (applied and constraints) are known. However, when the constraint forces are unknown, the Lagrange and Hamilton principles are more suitable than the Newton–Euler formalism. In fact, the two latter formulations use the D’Alembert principle, also known as the virtual work, to neglect the constraint forces in the development of the EOM. Moreover, they can be easily expressed in generalized independent coordinates, which is more complex in the **Newton–Euler formulation** [31]. The Newton–Euler and Lagrange formalisms are introduced in this subsection since they are the most employed in the case of reduced-order models [5,10].

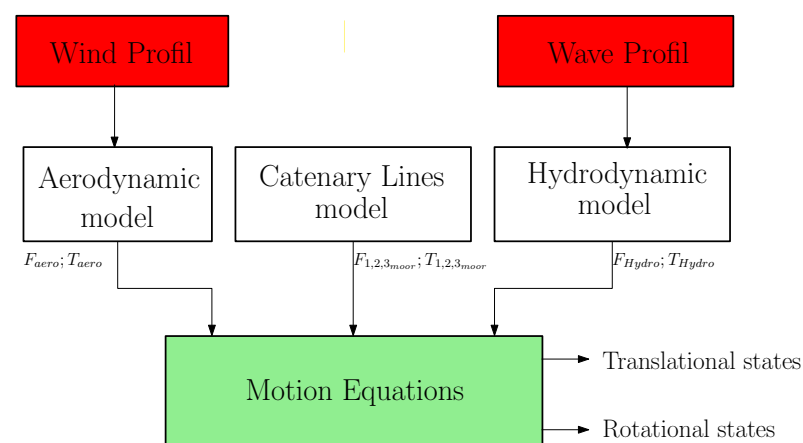


Figure 2. Module scheme of the mechanical structure model.

2.1.1. Newton–Euler Formulation

As its name indicates, the Newton–Euler EOM uses the Newton equation to express the displacements of translation and the Euler equation for those of rotation. According to [32], for the one-body mechanical system, the Newton–Euler EOM can be expressed as

$$\begin{cases} F^a + F^r = ma \\ L^a + L^r = I\alpha + \omega I\omega \end{cases} \quad (1)$$

where m and I are the mass and inertia, a is the acceleration of the mechanical system while ω is its angular velocity, F^a and L^a are the applied forces and loads, and F^r and L^r are the constraint forces and loads.

For mechanical systems that are easily represented in Cartesian coordinates and whose applied and constraint forces are known, the Newton–Euler EOM gives an intuitive and clear understanding of the body displacements. However, when the system becomes more complex with multiple bodies, interactions between each other, several external forces and non-intuitive coordinate variables, the Newton–Euler EOM becomes difficult to derive. However, in [32], a method is proposed for the Newton–Euler formalism to consider generalized coordinates and neglect the constraint forces by employing the virtual work principle of D’Alembert. This latter method has been applied to the reduced FOWT model in [8].

Writing (1) for a multi-body mechanical system, one can write,

$$\begin{cases} F_i^a + F_i^r = m_i a_i \\ L_i^a + L_i^r = I_i \alpha_i + \tilde{S}(\omega_i) I_i \omega_i \end{cases} \quad (2)$$

where i denotes one body of the system, and \tilde{S} is the cross-product operator defined as $\tilde{S} = \dot{S}S^T$, where S is the rotation tensor.

Defining the angular and translation accelerations as a function of a defined generalized coordinate vector q :

$$\begin{cases} a_i(q, \dot{q}) = \dot{v}_i(q, \dot{q}) = \frac{\partial v_i(q, \dot{q})}{\partial \dot{q}} \ddot{q} + \frac{\partial v_i(q, \dot{q})}{\partial q} \dot{q} = J_{t,i}(q, \dot{q}) \ddot{q} + \bar{v}_i \\ \alpha_i(q, \dot{q}) = \dot{\omega}_i(q, \dot{q}) = \frac{\partial \omega_i(q, \dot{q})}{\partial \dot{q}} \ddot{q} + \frac{\partial \omega_i(q, \dot{q})}{\partial q} \dot{q} = J_{r,i}(q, \dot{q}) \ddot{q} + \bar{\alpha}_i(q, \dot{q}) \end{cases} \quad (3)$$

where v is the velocity vector, \bar{v} is the local velocity, J_t is the translational Jacobian that transforms the translational kinematics of body i , originally described in the inertial coordinate system, into the space of minimal coordinates. The same approach for the rotational kinematics with the rotational Jacobian J_r .

Replacing (3) into (2), the Newton–Euler EOM can be rewritten as,

$$\begin{bmatrix} m_i J_{t,i} \\ \dots \\ I_i J_{r,i} \\ \dots \end{bmatrix} \ddot{q} + \begin{bmatrix} m_i \dot{J}_{t,i} \dot{q} \\ \dots \\ I_i \dot{J}_{r,i} \dot{q} + \tilde{S}(\omega_i) I_i \omega_i \\ \dots \end{bmatrix} = \begin{bmatrix} F_i^a \\ \dots \\ L_i^a \\ \dots \end{bmatrix} + \begin{bmatrix} F_i^r \\ \dots \\ L_i^r \\ \dots \end{bmatrix} \quad (4)$$

Using D’Alembert’s principle, the constraint forces and moments can be suppressed to obtain the following system for the Newton–Euler EOM,

$$M(q) \ddot{q} + k(q, \dot{q}) = p(q, \dot{q}), \quad (5)$$

where M is the total mass matrix, k is the Coriolis, gyroscopic and centrifugal forces, and p is the applied forces and torques.

2.1.2. Lagrangian Formulation

The Lagrangian formulation differs from the Newton–Euler one with the expressions of the potential energy V and the kinetic energy T . From these two energies, the Lagrangian operator L is defined as,

$$L(q_i, \dot{q}_i) = \sum_{i=1}^N (T(\dot{q}_i) - V(q_i)) \quad (6)$$

Then, the first-kind Lagrange EOM are obtained after solving the following equation for each generalized coordinate q ,

$$\frac{d}{dt} \left(\frac{\partial L}{\partial \dot{q}_i} \right) - \frac{\partial L}{\partial q_i} = Q_i \quad (7)$$

where Q is the generalized forces/torque vector.

If Q is exclusively composed of conservative forces that cannot be expressed as a gradient of potential energy, the D'Alembert principle can be applied to express a particular and less general case of the first-kind Lagrange EOM, named the second-kind Lagrange EOM,

$$\frac{d}{dt} \left(\frac{\partial L}{\partial \dot{q}_i} \right) - \frac{\partial L}{\partial q_i} = 0 \quad (8)$$

The Lagrange EOM has many advantages over the Newton–Euler equations such as its simplicity of the equations, the ability to add system variables as generalized coordinates, and the capacity to ignore constraint forces with appropriate generalized coordinates. In [31], the comparative conclusion on both mechanical approaches is given: “*In contrast to Newtonian mechanics, which is based on knowing all the vector forces acting on a system, Lagrangian mechanics can derive the equations of motion using generalized coordinates without requiring knowledge of the constraint forces acting on the system. Lagrangian mechanics provide a remarkably powerful and incredibly consistent approach to solving the equations of motion in classical mechanics, which is especially powerful for handling systems that are subject to holonomic constraints.*”

2.2. Aerodynamic Models

The possibility of aerodynamic models is numerous. The choice mainly depends on the required accuracy and the computational time constraint. Different theories have been proposed in the literature for classical wind turbines, which are briefly reviewed below.

2.2.1. CFD Methods

CFD methods are often based on Navier–Stokes or Euler equations to provide one of the most powerful and realistic tools for wind turbine flow field modeling. It has the ability to numerically solve the complex aerodynamic flow at the cost of expensive computation time. For detailed analysis and advanced designs, the CFD is the most suitable choice for its fidelity to reality. However, for control development or preliminary platform designs, the CFD method is prohibited since the details are not relevant for such applications, and the expensive computation time slows down the design process.

2.2.2. Blade Element Momentum (BEM) Theory

Originally developed by Rankine and Froude, the BEM theory is the most common theory for wind turbine aerodynamic models. It is based on the momentum theory whose particularity is to consider the rotating blade as an actuator disc combined with the Blade Element (BE) theory to divide the total blade into several small parts. It was developed to compute the aerodynamic loads on the classical onshore wind turbines through the computation of the drag and lift forces in several sections of the blades. Depending on the number of sections considered, the calculation time can increase considerably, making it unsuitable for controller design. BEM theory has been used in the AeroDyn module [33] of OpenFAST and Bladed aerodynamic code too.

2.2.3. Simplification of BEM Theory

The idea is to perform the BEM theory method offline for different operating points depending on the tip-speed ratio λ and the blade pitch angle β of the wind turbine. Lookup tables could be extracted to generate the aerodynamic power coefficient $C_p(\lambda, \beta)$ and the

aerodynamic thrust coefficient $C_t(\lambda, \beta)$. Then, the axial aerodynamic force F_A and torque M_A can be expressed as,

$$F_A = \frac{1}{2} \rho A_r C_t(\lambda, \beta) v_{rel}^2 \quad (9)$$

$$M_A = \frac{1}{2} \rho A_r \frac{C_p(\lambda, \beta)}{\omega_r} v_{rel}^3 \quad (10)$$

where ρ is the air density, A_r is the disc rotor area created by the rotating blades, ω_r is the rotor speed and v_{rel} is the relative wind speed. The relativity of the wind speed in the case of the FOWT is explained further. This aerodynamic model has been widely used in the case of reduced-FOWT models since it presents a good compromise between accuracy and computational time cost.

2.2.4. Free Vortex Wake (FVW) Theory

The FVW theory is part of the Vortex Wake theory with the rigid wake and prescribed wake model. It has the advantage of directly determining the vortical induction at each blade element, while the BEM theory computes the average induction. Moreover, it presents better efficiency than the CFD method with a higher resolution time than the BEM theory. This is the main reason why the BEM theory is more widely adopted in the literature. Another reason is that the FVW are commonly used for the analysis of the wake propagation phenomena when the wind crosses the rotating blade. From one wind turbine's point of view, these phenomena could be neglected, while for wind farms, it is of great interest since each wind turbine modifies the wind flow to the others. The AeroDyn code proposes the FVW method for the computation of aerodynamic loads. The Wake Induced Dynamics Simulator (WInDS) was developed at the University of Massachusetts and used the FVW method [34] as well.

Other theories exist in the literature, taking advantage of some of the above theories but having the disadvantages of others [35].

2.2.5. The Impact of the Floating Structure on the Aerodynamic Model

In the case of floating wind turbines, the wind speed perceived by the blades is not the exact wind speed. In fact, the six degrees of freedom (DOFs) created by the floating moving platform induce movements at the blade location. For example, if the FOWT is pitching forward against the wind speed vector, a relative wind speed higher than the actual wind speed is caught by the blade. Therefore, it is necessary to take into account all the six DOFs for high-fidelity models, while for a reduced-order model, the surge displacement and the pitch angle are those which impact most of the FOWT movements [36]. Furthermore, for a fixed reference frame, the relative wind speed captured by the blades can be written as

$$v_{rel} = v_{wind} + v_{surge} + v_{pitch} = v_{wind} + v_{surge} + d\dot{\alpha}\cos(\alpha) \quad (11)$$

2.3. Hydrodynamic Models

The hydrodynamic model allows the modeling of linear and nonlinear effects of the interactions between a body and the fluid in which it is immersed. It is a domain where several effects depend on the type of floating structure but also on the characteristics of the waves, such as its period and amplitude. In most of the hydrodynamic models, mooring line dynamics are not considered, but it is another model block. Instead, the hydrodynamic model considers the hydrostatic force combined with several wave forces. Thus, the literature proposes two types of possible representations of the wave forces while the hydrostatic is generally the same for all models. Each representation can be associated with either of the two models below:

1. The linear potential flow theory in the time domain with the Cummins equations splits the mathematical problems in three with radiation, hydrostatic and diffraction problems.

2. The viscous effect theory with the quadratic Morison equations for the drag and inertia forces combined.

The following paragraphs describe the two theories.

2.3.1. Linear Potential Flow in Time-Domain for the Hydrodynamic Model

The time-domain motion equations of the hydrodynamic model in the case of the linear potential flow are represented by the Cummins equation in (12) itself based on Newton's motion equation:

$$F_{ext} = M\ddot{x} = (M + A_\infty)\ddot{x}(t) + \underbrace{\int_0^t K_R(t-\tau)\dot{x}(\tau)d\tau}_{F_{rad}} + \underbrace{Cx(t)}_{F_{hyd-sta}} \quad (12)$$

where:

- M is the total mass and inertia matrix of the entire system on a predefined frame. This matrix does not include the added masses in this representation.
- A_∞ is the infinite added mass that gives the floater's instantaneous response to an acceleration. Its value can be computed in a preprocessing step with BEM software. As an example, the WAMIT commercial code BEM WAMIT could provide the mass added at different periods for all DOFs considered.
- x is the body states containing the surge, sway, heave, roll, pitch and yaw degrees of freedom.
- K is the retardation function and fluid memory also known as the impulse response function, with τ as a dummy time variable. $K(t)$ is computed from the frequency domain equation such as

$$K(t) = \frac{2}{\pi} \int_0^\infty B(\omega) \cos(\omega t) d\omega \quad (13)$$

where B is the radiation-damping matrix, and ω the angular frequency of the incident wave.

- C is the restoring hydrostatic constant matrix. Its values can be computed based on (14) or with BEM software commercial software such as WAMIT, Ansys AQWA or with the open-source BEM software NEMOH [37].

$$C = \begin{bmatrix} 0 & 0 & 0 & 0 & 0 & 0 \\ 0 & 0 & 0 & 0 & 0 & 0 \\ 0 & 0 & \rho g A_0 & 0 & -\rho g \iint_A x dA & 0 \\ 0 & 0 & 0 & \rho g \iint_{A_0} y^2 dA + \rho g V_0 z_{COB} & 0 & 0 \\ 0 & 0 & -\rho g \iint_{A_0} x dA & 0 & \rho g \iint_{A_0} x^2 dA + \rho g V_0 z_{COB} & 0 \\ 0 & 0 & 0 & 0 & 0 & 0 \end{bmatrix} \quad (14)$$

- F_{ext} is the external hydrodynamic forces without consideration of the mooring line forces. Depending on the accuracy of the model, the external forces can differ from one model to another. Commonly, the Froude–Krylov force for the diffraction phenomena and the buoyancy force are part of the external forces. Note that the radiation force and the hydrostatic force are already considered in the Cummins Equation (12), with the convolution integral representing the radiation damping of the wave and the hydrostatic restoration matrix.

To conclude, the Cummins equation can be used as a hydrodynamic model that takes into account different hydrodynamic effects except for the viscous one. One drawback of the linear potential flow theory is that it requires external BEM software for the computation of the added masses, the radiation and the hydrostatic restoring matrices.

2.3.2. Viscous Hydrodynamic Theory

This second theory is usually employed in the FOWT to consider the drag and inertia phenomena of the submerged body. The classical equation to describe this theory is the nonlinear Morison equation. It gives the axial force $F_{H,i}$ on each discretized section i of the floating cylinder in function of the inertia force $F_{inertia}$ and the drag force F_{drag} such as

$$F_{H,i} = F_{inertia,i} + F_{drag,i} = (1 + C_a)\rho_w\pi\frac{D_i^2}{4}a_w + \frac{1}{2}\rho_w C_d D_i v_w |v_w| \quad (15)$$

where

- C_a and C_d are the added mass and drag coefficients that can be obtained from the literature depending on the cylinder characteristics [38]
- D_i is the diameter of the considered cylinder section i
- v_w and a_w are, respectively, the unperturbed water velocity and acceleration.

The overall force is obtained by integrating over the total length of the cylinder. The Morison equation takes into account the drag load on the floating substructure. However, it neglects the impact of the floating body on the incident wave.

Each of these two theories is subject to validity conditions that are defined based on the product of the wavenumber k of the incident waves to the floating platform radius a , known as the diffraction parameter, and on the period number, also called the Keulegan–Carpenter (KC) number. The first parameter gives an indication of the impact of diffraction phenomena, while the KC parameter describes the importance of the drag phenomena over the inertia one. For high floater diameter, the wave diffraction phenomena must be considered. For small KC, the inertia effect is more relevant than the drag one.

For floating offshore wind turbines, it seems that the appropriate mid-fidelity model is in the middle of both theories. The drag load, as well as the radiation, diffraction should be taken into account for realistic models. Thus, a suitable floating offshore wind turbine's hydrodynamic model should mix the linear potential theory with the viscous theory. Thus, such model will consider the added masses, the radiation, the diffraction and the hydrostatic restoring effects on the left-hand side of the time-domain Cummins equation. On the right-hand side with the external force F_{ext} , the Morison equations could account for the drag and inertia forces combined with the buoyancy and weight forces for the static equilibrium in still-water.

2.4. Mooring Line Models

The mooring lines are a set of lines that connect the floating platform to the seabed. They are used in the FOWT to keep the floater in a specific area in the presence of wind, waves and also wave currents in the case of a float that is deeply submerged in water, such as spar-buoy float. For the TLP, the mooring lines provide stability to the platform by reducing all the six DOF. Depending on the complexity, three models are commonly used in the literature: static, quasi-static and dynamic models.

2.4.1. Static Model

The static model is a linear model that neglects the mooring inertia and damping. Only the pretensioned force $F_{L,0}$ and the restoring 6-by-6 matrix C_L represent the total load forces. For three mooring lines, the total static force can be written as

$$F_L^{1,2,3} = F_{L,0}^{1,2,3} - C_L q \quad (16)$$

where q is the six DOFs of the floating platform. The values of the restoring matrix C_L are obtained from the linearization of the external quasi-static or dynamic models presented next.

2.4.2. The Quasi-Static Model

When chosen, the quasi-static model usually refers to the MAP++ code from the National Renewable Energy Laboratory (NREL) of America [39]. This code assumes that the platform is subject to small displacements in the six DOFs; thus, it neglects the dynamic effects, the added mass, the damping and the inertia produced by the mooring system. The quasi-static model computes the cable tension force T_e of the lines at each simulation iteration in function of the fairlead displacements of the floating platform. Between each time step, no platform motion is considered, i.e., the platform is static. MAP++ expressed the horizontal and vertical positions of the fairlead x_F and z_F , respectively, in function of the horizontal and vertical components of the effective mooring line tensions at the fairlead location, H_F and V_F , respectively. Two sets of equations are possible depending on if a part of the line rests on the seabed or not. Figure 3 illustrates the different variables when no line rests on the seabed.

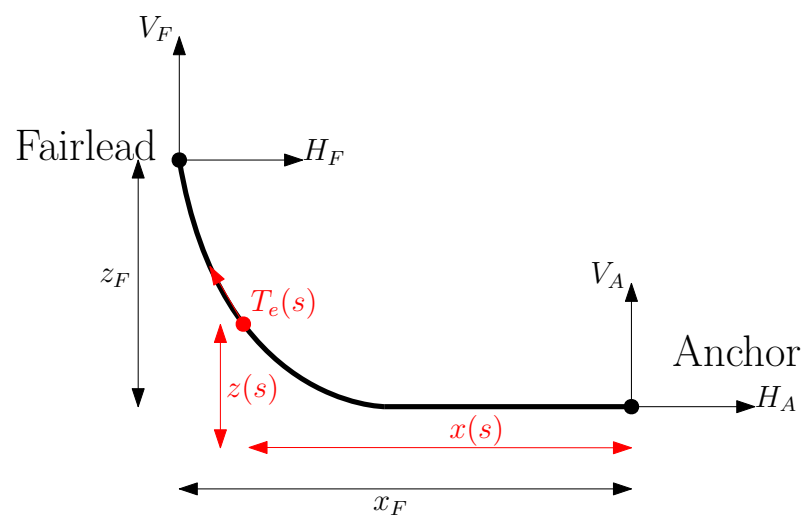


Figure 3. One mooring line representation in 2D for quasi-static modeling.

If the total length of the line is floating, the following expressions for x_F and z_F can be expressed:

$$\begin{cases} x_F(H_F, V_F) = \frac{H_F}{\omega} \left(\ln \left[\frac{V_F}{H_F} + \sqrt{1 + \left(\frac{V_F}{H_F} \right)^2} \right] - \ln \left[\frac{V_F - \omega L}{H_F} + \sqrt{1 + \left(\frac{V_F - \omega L}{H_F} \right)^2} \right] \right) + \frac{H_F L}{EA} \\ z_F(H_F, V_F) = \frac{H_F}{\omega} \left[\sqrt{1 + \left(\frac{V_F}{H_F} \right)^2} - \sqrt{1 + \left(\frac{V_F - \omega L}{H_F} \right)^2} \right] + \frac{1}{EA} (V_F L - \frac{\omega L^2}{2}) \end{cases} \quad (17)$$

If a part of the line does not float, these expressions are used:

$$\begin{cases} x_F(H_F, V_F) = L_B + \frac{H_F}{\omega} \ln \left[\frac{V_F}{H_F} + \sqrt{1 + \left(\frac{V_F}{H_F} \right)^2} \right] + \frac{H_F L}{EA} \\ \quad + \frac{C_B \omega}{2EA} \left[-L_B^2 + \left(L_B - \frac{H_F}{C_B \omega} \right) \text{MAX} \left(L_B - \frac{H_F}{C_B \omega}, 0 \right) \right] \\ z_F(H_F, V_F) = \frac{H_F}{\omega} \left[\sqrt{1 + \left(\frac{V_F}{H_F} \right)^2} - \sqrt{1 + \left(\frac{V_F - \omega L}{H_F} \right)^2} \right] + \frac{1}{EA} \left(V_F L - \frac{\omega L^2}{2} \right) \end{cases} \quad (18)$$

where $L_B = L - (V_F/\omega)$ is the total unstretched portion of one mooring line that rests on the seabed with L as the total unstretched length, ω the apparent weight in the fluid per unit length, EA is the extensional stiffness and C_B is the seabed static-friction drag coefficient.

The two previous equations are solved with the Newton–Raphson iteration tool for the unknown fairlead effective positions and tensions, respectively x_F , z_F , H_F and V_F .

For the horizontal and vertical components of the effective tension at the anchor location H_A and V_A , respectively, their expressions are as follows when a portion of the line rests on the seabed:

$$\begin{cases} H_A = H_F \\ V_A = V_F - \omega L \end{cases} \quad (19)$$

When the line is totally floating, these expressions are used

$$\begin{cases} H_A = \text{MAX}(H_F - C_B \omega L_B, 0) \\ V_A = 0 \end{cases} \quad (20)$$

Once the effective tension components of the fairlead and the anchor are obtained, the effective tension can be expressed as follows when no part of the line is in contact with the seabed:

$$T_e(s) = \sqrt{H_F^2 + (V_A + \omega s)^2} \quad (21)$$

When a portion is in contact with the seabed:

$$T_e(s) = \begin{cases} \text{MAX}(H_F + C_B \omega(s - L_B), 0), & \text{for } 0 \leq s \leq L_B \\ \sqrt{H_F^2 + (\omega(s - L_B))^2}, & \text{for } L_B \leq s \leq L \end{cases} \quad (22)$$

2.4.3. Dynamic Model

Dynamic models consider the nonlinear effects of the mooring lines such as the inertia, added mass and damping. MoorDyn [40] is a dynamic mooring model developed by Matthew Hall. It considers many effects such as the internal axial stiffness and damping forces, the couple weight and buoyancy forces, the inertia and drag forces and the vertical spring-damper forces [40]. The MoorDyn code allows modeling the line with different sections of different materials to add a clumped mass at any location of the line and to interface the dynamic model to MATLAB/Simulink or other simulation software. For the sake of brevity, the equations are not mentioned in this paper.

The quasi-static model presents a suitable compromise between accuracy and numerical resolution time. It is also the most famous mooring line model for FOWT model codes such as in [5,9]. In order to reduce the computational time, the quasi-static model can be run offline for different displacements x_F and z_F around the static equilibrium in still-water and to upload the obtained tension components H_F and V_F in lookup tables or to approximate them with curve fitting methods. It is important to mention that for TLP-based platform with constantly tensioned mooring lines, the model can be expressed with spring equations as in [4].

2.5. Drivetrain Models

The drivetrain shaft is usually composed of two parts separated by a gearbox: the low-speed shaft at the rotating blade side and the high-speed shaft at the generator side. To model the shaft that connects the rotating blade to the generator, several models can be chosen depending on the modeling objectives. In fact, for control design and first step modeling, neglecting the friction torque, the one-mass drivetrain model expressed as (23), where two shafts are rigid, can be used.

$$\dot{\omega}_r = \frac{1}{J_r} \left(\frac{P_A}{\omega_r} - T_g \right) \quad (23)$$

where ω_r is the low-speed shaft speed, named rotor angular speed, J_r is the rotor inertia, P_A is the aerodynamic power and T_g is the generator torque.

To consider the shaft torsion, the two-mass drivetrain model, where one shaft is flexible, can be used. According to [41], the two-mass drivetrain model with the flexible

low-speed shaft can be expressed as (24). However, the use of such a model will inevitably increase the complexity of the control design.

$$\begin{aligned}\dot{\omega}_r &= \frac{1}{J_r} \left(\frac{P_A}{\omega_r} - k_r(\Delta\theta_r) - b_r(\dot{\theta}_r) \right) \\ \dot{\omega}_g &= \frac{1}{J_g} \left(-T_g + \frac{k_r}{N_{GR}}(\Delta\theta_r) + \frac{b_r}{N_{GR}}(\dot{\theta}_r) \right)\end{aligned}\quad (24)$$

where k_r is the stiffness constant, b_r is the damping constant, θ_r is the low-speed shaft angle, ω_g is the generator angular speed, J_g is the generator inertia and N_{GR} is the gearbox ratio between the two shafts.

2.6. Wind Profile

Realistic wind profiles are composed of two parts: an undisturbed wind signal and a turbulent wind signal. They can be created in a preprocessing step using external codes such as TurbSim [42] from NREL.

Several undisturbed wind profiles can be generated on TurbSim such as

- The logarithmic wind profile (25), which calculates the average wind speed at a desired height z relative to the water level based on a known wind speed at a reference height z_{ref} , where $z_{ref} \neq z$:

$$\bar{u}(z) = \bar{u}(z_{ref}) \frac{\ln\left(\frac{z}{z_0}\right) - \phi_m}{\ln\left(\frac{z_{ref}}{z_0}\right) - \phi_m} \quad (25)$$

where \bar{u} is the mean wind speed, z_0 is the input surface roughness and ϕ_m a function that depends on the gradient Richardson stability parameter.

- The power-law wind profile in (26) that computes the average wind speed at a predefined height depending on the exponent of the power law.

$$\bar{u}(z) = \bar{u}(z_{ref}) \left(\frac{z}{z_{ref}} \right)^{\alpha_{PL}} \quad (26)$$

where α_{PL} is the input power-law exponent parameter.

- The IEC wind profile that uses the power-law wind profile on the rotor-disk and the logarithmic profile outside.
- Low-level jet wind profile that generates wind profiles in different directions while the previous one generates wind profiles in one direction. It is based on the Chebyshev polynomials as follows:

$$\bar{u}(z) = \sum_{n=0}^{10} c_n T_n(z) \quad (27)$$

where T_n is the n^{th} order of the Chebyshev polynomial, and c_n is the Chebyshev coefficient.

The turbulence models of the wind profile are based on spectral representations because of the chaotic turbulence phenomena. In the TurbSim code, multiple spectral models are available (IEC Kaimal, IEC Von Karman, Riso Smooth-Terrain, etc.). For the sake of brevity, the two most famous spectral are presented: the Kaimal and Von Karmal spectra.

2.6.1. Kaimal Spectrum

The Kaimal spectrum is defined as follows

$$S_K(f) = \frac{4\sigma_K^2 L_K / \bar{u}_{hub}}{(1 + 6f L_K \bar{u}_{hub})^{5/3}} \quad (28)$$

where f denotes the frequency, σ_K is the wind standard deviation, L_K is an integral scale parameter defined in (29), and \bar{u}_{hub} is the mean wind speed at hub height.

$$L_K = \begin{cases} 8.10\phi_U, & K = U \\ 2.70\phi_U, & K = V \\ 0.66\phi_U, & K = W \end{cases} \quad (29)$$

where ϕ_U is the turbulence scale parameter.

2.6.2. Von Karman Spectrum

The Von Karman spectrum is defined as follows,

$$S_K(f) = \begin{cases} \frac{4\sigma_K^2 L / \bar{u}_{hub}}{(1+71(fL/\bar{u}_{hub})^2)^{5/6}}, & \text{for } K = U \\ \frac{2\sigma_K^2 L / \bar{u}_{hub}}{(1+71(fL/\bar{u}_{hub})^2)^{11/6}} (1 + 189(fL/\bar{u}_{hub})^2), & \text{for } K = V, W \end{cases} \quad (30)$$

where the integral scale parameter L is defined as $L = 3.5\phi_U$.

2.7. Wave Profile

In order to have realistic simulations, it is essential to have wave profiles close to what can be encountered in reality. Thus, three cases of wave modeling are possible:

1. Regular waves: the free surface wave elevation, commonly written as η , is defined by the linear airy wave theory as

$$\eta(x, t) = a \cdot \cos(kx - \omega t) \quad (31)$$

where a is the wave amplitude in meters, k is the angular wavenumber in radians per meter, x is the horizontal position in meter, t is the time in seconds and ω is the angular frequency. This expression is very limited since the waves are never sinusoidal. The amplitude above the still water level, called the crest, is always higher than the absolute amplitude under the still water level called the trough. In fact, the free wave elevation is mainly due to the wind that acts directly on the crest rather than the trough.

2. Stokes waves: elaborated by Georges Stokes for the model of free elevation waves in deep water, it models the free elevation η as nonlinear and periodical surface waves. It is based on the second-order and third-order theories, while the first-order version of the Stokes wave theory is actually the airy wave theory [43].
3. Irregular waves: this model is the most realistic one. In fact, the natural free wave elevation is a random and confusing phenomenon with multiple wavenumbers, frequencies and amplitudes at one location x . Hence, the irregular free elevation can be written as a superposition of multiple regular waves such as

$$\eta(x, t) = \sum_{i=1}^N a_i \cos(k_i x - \omega_i t + \epsilon_i) \quad (32)$$

where N is the number of superposed monochromatic regular waves, and ϵ is a random angle. To obtain a realistic and logical combination of the N amplitudes a_i , a wave spectrum model is used, and the amplitudes are defined as:

$$a_i = \sqrt{2S(\omega_i)\Delta\omega} \quad (33)$$

As for the wind, different spectra exist, the most famous of which are the Pierson–Moskowitz (PM) and the Joint North Sea Wave Project (JONSWAP) spectrum. The first spectrum is defined as follows

$$S_{PM}(\omega) = \frac{5}{16} H_s^2 \omega_p^4 \omega^{-5} \exp\left(-\frac{5}{4} \left(\frac{\omega}{\omega_p}\right)^{-4}\right) \quad (34)$$

where ω_p is the peak angular frequency, and H_s is the significant wave height. The JONSWAP is near to the PM spectrum, but its validity is better in a fetch limited context:

$$S_J(\omega) = A_\gamma S_{PM}(\omega) \gamma^A \quad (35)$$

where A_γ is a normalizing factor function of γ , which is the peak shape parameter, and A is a dummy variable whose expression is given as

$$A = \exp\left(-\left(\frac{\frac{\omega}{\omega_p} - 1}{\sigma\sqrt{2}}\right)^2\right) \quad (36)$$

where σ is a spectral width parameter.

3. COMs of FOWTs

COMs are part of the reduced FOWT models and have been developed for the design of model-based controllers. This study is focused on the nonlinear time-domain COMs for the establishment of novel nonlinear algorithms for the control of FOWTs. Three COMs have been selected from the literature for their nonlinearity, their ability to be reproduced and for their accuracy compared to the high-fidelity code OpenFAST. The first nonlinear COM is the 5 MW TLP-based FOWT in [4], which is called the *Betti model*. The second nonlinear COM is the 5 MW spar-buoy FOWT proposed in [5] in its more reduced version in [8], which is called the *Lemmer model*. The last nonlinear COM is the 5 MW semi-submersible-based FOWT proposed in [9], which is called the *Homer model*.

3.1. Betti Model

The TLP is known for its great mechanical stability based on tensioned mooring lines stretched on the seabed. The design of the platform increases the buoyancy of the floater, and the tension forces of the cables retain it. This constant balance makes it possible to limit the oscillation movements at the cost of significant stress on the lines. This model described the FOWT with seven states: surge, heave, pitch and their respective velocities, as well as the rotor speed. Furthermore, there are two control inputs, i.e., the generator torque and the collective blade pitch angle. The platform and the wind turbine are aligned with the wind. In other words, the rotor axis vector and the wind vector are collinear, and the yaw error angle is considered to be zero. These simplifications make possible the representation of the FOWT in 2D. All elements of the wind turbine structure are considered rigid. The EOM are expressed with the Lagrangian approach. The drivetrain is modeled as a rigid one-mass drivetrain shaft. Three aerodynamic forces are considered and applied at the centers of mass of the nacelle, the rotor-hub-blade assembly and the tower. These are expressed on the known Bernoulli equations from the BEM theory. The hydrodynamic equations use the viscous theory with the Morison equation that expresses the inertia and drag forces of the submerged TLP. It is combined with the hydrostatic Archimède equation for flotation force expressions. The last module is the mooring line dynamic, which is modeled based on spring equations. The major characteristics of the Betti COM are summed up in Table 1.

Table 1. Model blocks comparison of the three COMs.

Models	Betti	Lemmer	Homer
States	6	6	16
Command	2	2	2
EOM	Lagrange	Newton–Euler	Newton-Euler
Aero. Model	BEMT	BEMT	BEMT
Hydro. Model	Morison equations, Hydrostatic and Buoyancy	Linear hydrostatic and damping	Morison equations, Buoyancy and Froude–Krylov equation
Moor. Model	Spring equations	Linear stiffness	Polynomial approx.
Shaft Model	One-mass	One-mass	Two-mass

3.2. Lemmer Model

In this model, the very large cylinder is used to make the center of gravity much lower in the water than the center of buoyancy for stabilizing the wind turbine. For this, the heavy ballast mass will introduce a higher weight to the lower structure than the higher one. In addition, a small volume is in contact with the free surface. Thus, fewer wave forces are expected, which increases the stability of the platform. As indicated in Table 1, the Lemmer model is expressed with six states: surge and pitch displacements with their related velocities and the nacelle displacement due to tower-top fore-aft flexibility, i.e., perpendicular to the rotor plane with its velocity. Note that, compared to the two previous models, the tower flexibility is considered in the Lemmer model while all the other bodies are considered to be rigid. The control inputs are the generator torque and the blade pitch angle. No misalignment between the waves and the wind is considered. Assuming that the wind is perpendicular to the axis of the blades, the wind turbine is modeled in 2D as the Betti model. The equations of motion are expressed with the Newton–Euler mechanical formalism from [32]. Each body in the system has its own frame, and the applied forces are expressed in their reference frame, while the constraint forces are neglected based on the D’Alembert principle. Everything is finally expressed in the inertial reference frame, whose origin is the center of the platform’s waterline in still water. The aerodynamics are modeled with the simplified BEM theory at the center of the rotor disc, i.e., at the hub location. In the selected version of the Lemmer models, the hydrodynamic model has been reduced to the hydrostatic restoring coefficients against the pitching angular displacements and the linear damping for surge and pitch DOFs, while the viscous theory has been neglected for the spar-buoy platform concept. In fact, the hydrodynamic model of this COM considers no incident waves, i.e., the FOWT is in still water. The mooring line model has been modeled only against the surge displacement with a linear stiffness coefficient. Other versions of this model have been published in the literature with more complex hydrodynamic models that consider the entire linear potential flow theory with diffraction and radiation phenomena combined with the Morison drag theory for the inertia and drag forces. Furthermore, the second-order wave dynamics have been modeled for accurate hydrodynamic representations. However, to the best of the author’s knowledge, no article has presented the Lemmer model in detail expected for the selected version of this study.

3.3. Homer Model

The semi-submersible platform is composed of three cylinders positioned at 120 degrees from each other, and this floater is an ideal solution from a logistical point of view for the assembly and installation of the wind turbine. Indeed, the vast majority of the assembly can be performed onshore. However, a large volume is in contact with the waves, which

makes it sensitive to water flows. This model adopts 16 states, which are the six DOFs of the platform, the rotor and generator angle and all the velocity of the aforementioned states. Compared with the 2D models above, this model is a 3D model of the FOWT, taking into account a possible wind-wave misalignment between each other and introducing a control input to the generator torque and blade pitch angle inputs: the nacelle yaw angle. The entire structure is considered rigid except for the drive train shaft modeled as a dual-mass model with torsional flexibility. The motion equations are expressed with Newton–Euler formalism. However, the inertia tensor is considered constant in the Homer model, which simplifies the frame transformations. This large simplification may be valid when rotor inertia is much smaller than the platform and tower inertia together. The aerodynamic module is based on the simplified BEM theory. The hydrodynamic model considers the viscous theory with the Morison equation, the diffraction phenomena with the Froude–Krylov equations combined with the buoyancy force. However, the hydrostatic effect has not been considered in the Homer model. The mooring lines are modeled as a polynomial approximation of the resulting forces obtained with the MAP++ quasi-static code. The vertical and horizontal forces are expressed for different heave and surge displacements to obtain a 3D surface. A position-dependent polynomial expression is obtained to generate the two forces rather than using MAP++ directly, which could increase the simulation time.

3.4. Control-Oriented Models Comparison

The three COMs have been reproduced on the Matlab/Simulink simulation tool in specific wind and wave conditions that correspond to their published research papers. Each of them is compared with the high-fidelity code OpenFAST. Developed by the NREL, OpenFAST can accurately describe the dynamics of the FOWT with a high fidelity. It contains 26 preconfigured wind turbines with 24 DOFs: two fore-aft and two side-to-side modes of the flexible tower, two flap modes and one edge mode per blade, one generator azimuth, one shaft torsion, the yaw bearing nacelle, two modes for the furl, three translations and three rotations for the platform. Different modules are connected to the main code to provide the aerodynamic, hydrodynamic and mooring lines forces and torques at each computation time, leading to a model of 44 states and 8 control inputs with 3 individual blade angles, the torque and power of an external generator model, the yaw and rate nacelle angle and the high-speed shaft breaking fraction.

3.4.1. Simulation Results

For each COM, its states and the corresponding OpenFAST states are plotted. From the obtained figures, the root-mean squared error (RMSE) and the standard deviation (STD) are denoted in Table 2. Furthermore, the reproduction complexity of the model is assessed based on the author's appreciation.

Table 2. Summary of simulation results.

Etats	RMSE			STD		
	Betti	Lemmer	Homer	Betti	Lemmer	Homer
Surge (m)	0.8034	4.0728	1.5205	1×10^{-4}	[-]	4×10^{-4}
Heave (m)	0.2020	[-]	0.5204	1×10^{-3}	[-]	2×10^{-3}
Sway (m)	[-]	[-]	0.4309	[-]	[-]	9×10^{-4}
Pitch (deg)	0.0309	1.6361	0.4753	2×10^{-4}	1.5×10^{-2}	4×10^{-4}
Roll (deg)	[-]	[-]	0.4409	[-]	[-]	1.5×10^{-3}
Yaw (deg)	[-]	[-]	0.6114	[-]	[-]	2.6×10^{-2}

Betti Model

The Betti model has been validated in open-loop with incremental wind steps that cover region 3. It is not mentioned in [4], but the wave height kinematic is not considered in

this validation, i.e., the model is validated in still-water. In Figure 4, the wind speed profile, the generator torque, the blade pitch angle, the translational surge, heave displacements and the rotational pitch angle are depicted and compared with OpenFAST code.

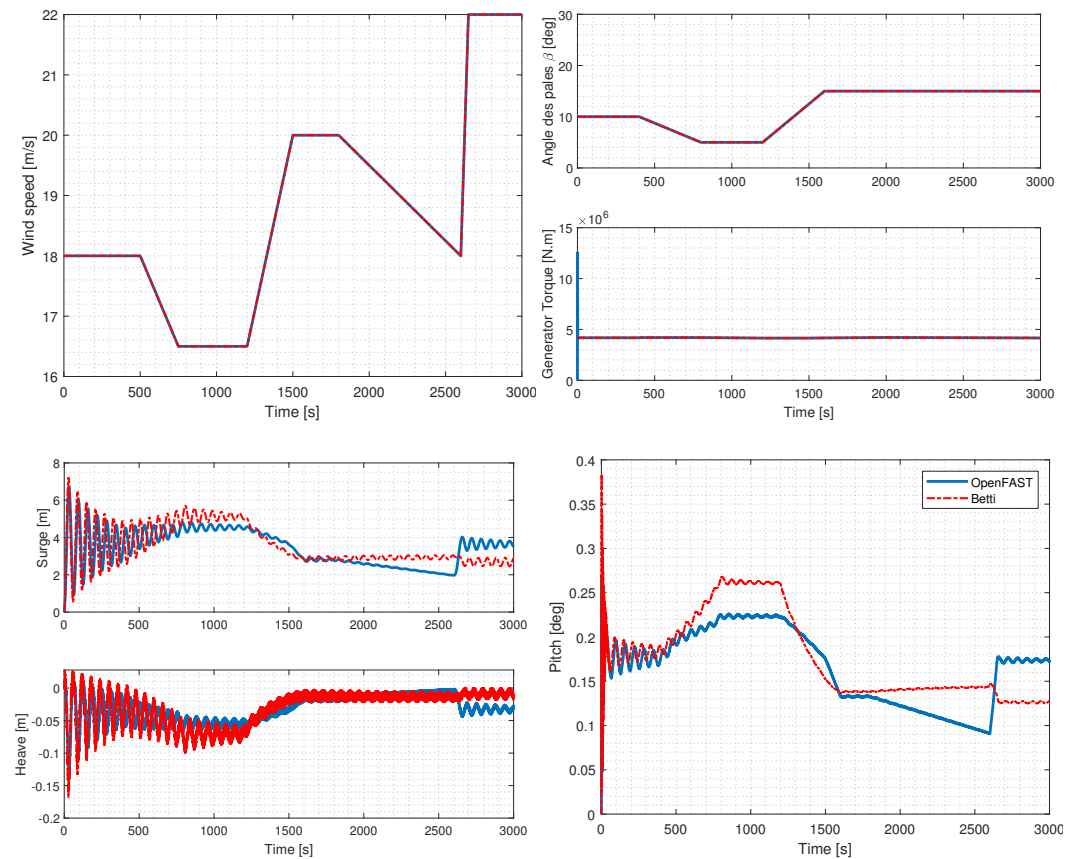


Figure 4. Simulation comparison following [4] conditions with OpenFAST code in blue and Betti model in red: wind speed profile (**top-left**), generator torque and blade pitch angle control inputs (**top-right**), surge and heave translational DOFs (**bottom-left**) and pitch angular DOF (**bottom-right**).

The produced surge, heave and pitch DOFs are relatively closed to OpenFAST code. Based on the author's analysis, the obtained results of [4], in open-loop, could not be obtained exactly. Furthermore, the hydrodynamic model cannot be completely assessed without wave kinematics. In fact, the Morison equations are dependent on the wave velocity and acceleration. Only the buoyancy forces are assessed in the hydrodynamic model.

Lemmer Model

The selected COM of the Lemmer model is developed in still-water conditions with wind speed that corresponds to region 2. The wind profile and the considered DOF are depicted in Figure 5 with a comparison to OpenFAST. The results show large errors for the three considered DOFs while keeping their global dynamics closed to OpenFAST. In this validation, it is important to emphasize that the OpenFAST code does not consider the wave kinematics; however, all the DOF are enabled.

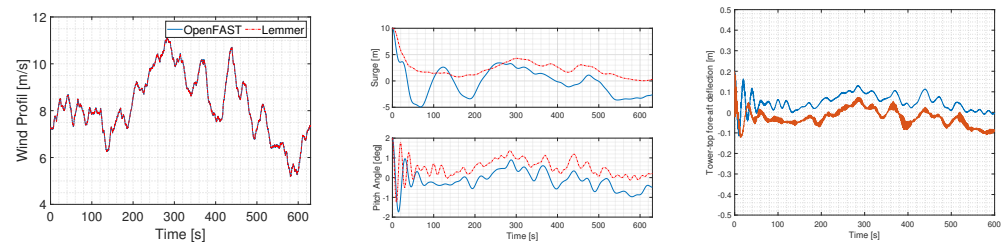


Figure 5. Simulation comparison following conditions of [8] with OpenFAST code in blue and Lemmer model in red: wind speed profile (left), surge and pitch translational DOFs (middle) and tower-top fore-aft deflection (right).

If the wave kinematics are added to the OpenFAST model and the wind speed profile is designed for region 3, the following results in Figure 6 are obtained. The wave kinematics add small oscillations at a higher frequency than the global dynamics of the considered DOFs. For the tower-top deflection, the realistic model shows a higher amplitude than the Lemmer model. However, the wind profile in Region 3 does not affect the model accuracy compared to the obtained results in Figure 5.

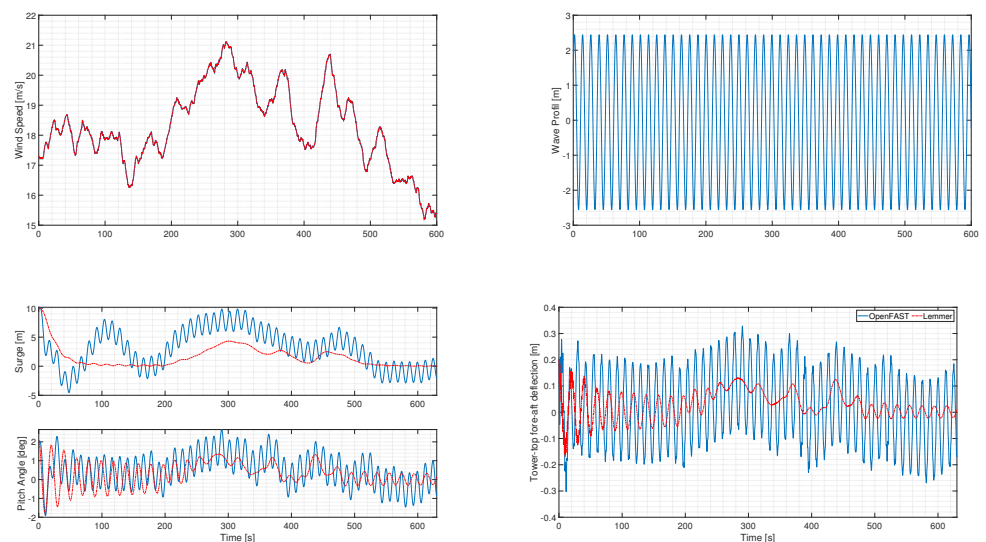


Figure 6. Simulation comparison in region 3 with OpenFAST code in blue and Lemmer model in red: wind speed profile (top-left), wave profile (top-right); surge and pitch translational DOFs (bottom-left) and tower-top fore-aft deflection (bottom-right).

Homer Model

This COM considers the three translational and the three angular DOFs of the floating platform. Furthermore, the validation has been performed with a 3D wind profile in region 3 with the consideration of the wave height kinematics. These two profiles with the simulation results are shown in Figure 7. The simulation results show a good agreement of the proposed COM with the OpenFAST for all considered DOF.

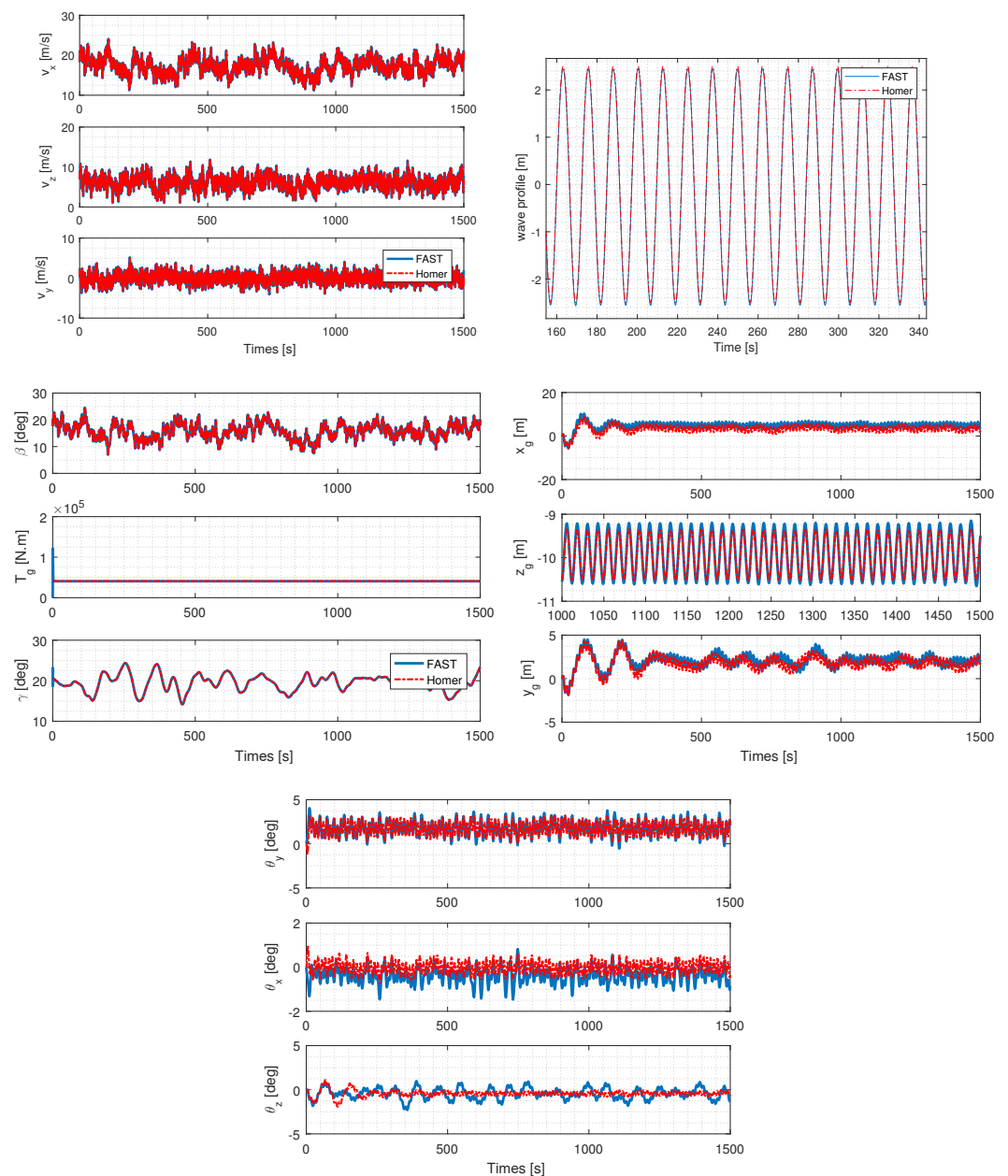


Figure 7. Simulation comparison following conditions of [9] with OpenFAST code in blue and Homer model in red: wind speed profile (**top-left**), generator torque and blade pitch angle control inputs (**top-right**), surge and heave translational DOFs (**bottom-left**) and pitch angular DOF (**bottom-right**).

Discussion

For a global comparison, the RMSE and the STD of the three COMs are given based on the simulation comparison in the same context as the author's papers. The smallest RMSE and STD mean the highest accuracy of the model compared to OpenFAST. The Betti COM shows good agreement with OpenFAST. Among the three models, it is the most accurate one for its considered DOFs, with an RMSE of 0.8034 and 0.2020 m for the surge and heave DOFs, respectively. However, the STD values show fewer deviations for the Homer model than for the two others. The Betti model has been validated on a non-turbulent wind profile. Furthermore, the model validation has been accomplished without a wave profile, meaning that only the hydrostatic phenomenon has been validated in these conditions, while the Morison equation has not been properly confirmed. However, the Lagrange formalism makes the model reproduction simple compared to the other models. The Lemmer model in

its most reduced form presents a powerful tool for the fast development of control designs. Despite its large errors compared to the other COMs, it conserves the global dynamics in Region 3 with wave kinematics that seem sufficient from the control point of view. In fact, for controllers that are highly robust to unmodeled dynamics, the Lemmer COM could be a competent alternative to more sophisticated COMs, especially control designers that are not familiar with fluidic dynamics and modeling. However, the model reproduction could be difficult if one wants to upgrade the force equations with more complex considerations. The Homer model is the most accurate model among the three selected COMs regarding the STD values. It is validated in realistic-environment conditions with turbulent and multi-directional wind profiles and wave kinematics. However, the number of DOFs considered makes the system equations more complex than the Lemmer and Betti models.

To conclude the simulation comparative analysis, the Betti model formulation is suitable for control designers that want to develop controllers on the TLP-based platform. Furthermore, this model can be easily reproduced without massive background in fluidic mechanics. To design control laws in a fast manner without strong knowledge of all the complexity of the FOWT system, the most reduced Lemmer model is suitable. Moreover, the simulation time is very small, which allows the use of this model for designing the model-based controllers such as the model predictive controller [20]. Furthermore, it is the only COM among the three presented models that considers the flexibility of the structure. If the control designers need to feed-forward DOFs other than the surge, heave and pitch displacements, the Homer model is a powerful candidate since all the six DOFs are available with accurate results. Moreover, the model is fully available in the literature with a clear understanding of the modeling equations.

4. Application Example: Model-Based Nonlinear Second-Order SMC Design

The Betti model is selected for the 5 MW TLP-based FOWT control design. First, the selected model is briefly presented in its original form. Then modifications of the aerodynamic equations are proposed in order to obtain fully analytical aerodynamic equations and to rewrite the model as an affine function in control. Based on that, a model-based twisting algorithm is designed to achieve the control objectives in region 3, which are presented in Section 4.2.

4.1. Betti COM for TLP-Based FOWT

According to [4], the Lagrange equation of motion for the FOWT can be expressed as

$$\mathbf{E}\dot{\mathbf{x}}_1 = \mathbf{F} \quad (37)$$

where \mathbf{x}_1 is the vector of the state variables expressed as (38), and \mathbf{E} is the coefficient matrix expressed as (39) and \mathbf{F} is the generalized force vector expressed as (40).

$$\mathbf{x}_1 = [\xi \quad v_\xi \quad \eta \quad v_\eta \quad \alpha \quad \omega]^T \quad (38)$$

$$\mathbf{E} = \begin{bmatrix} 1 & 0 & 0 & 0 & 0 & 0 \\ 0 & M_X & 0 & 0 & 0 & M_d \cos \alpha \\ 0 & 0 & 1 & 0 & 0 & 0 \\ 0 & 0 & 0 & M_Y & 0 & M_d \sin \alpha \\ 0 & 0 & 0 & 0 & 1 & 0 \\ 0 & M_d \cos \alpha & 0 & M_d \sin \alpha & 0 & J_{TOT} \end{bmatrix} \quad (39)$$

$$\mathbf{F} = \begin{bmatrix} v_\xi \\ Q_\xi + M_d \omega^2 \sin \alpha \\ v_\eta \\ Q_\eta - M_d \omega^2 \cos \alpha \\ \omega \\ Q_\alpha \end{bmatrix} \quad (40)$$

where ξ and v_{ξ} are the surge position and velocity, i.e., $\dot{\xi} = v_{\xi}$, η and v_{η} are the heave position and velocity, i.e., $\dot{\eta} = v_{\eta}$ and α and ω are the surge displacement and velocity, i.e., $\dot{\alpha} = \omega$. M_X , M_Y , M_d and J_{TOT} are constant values containing the masses, the added masses and the inertia of the FOWT bodies. Table VI of [4] provides the numerical values. $Q_{\xi,\eta,\alpha}$ are the generalized forces expressed in the generalized coordinate (ξ, η, α) , respectively.

The drivetrain shaft is modeled as a one-mass rigid shaft neglecting friction torque. Thus, the rotor speed dynamic is expressed as

$$\dot{\omega}_r = \frac{1}{\tilde{J}_r} (T_A - \tilde{T}_E) = \frac{1}{\tilde{J}_r} \left(\frac{P_A}{\omega_r} - \tilde{T}_E \right) \quad (41)$$

where ω_r is the rotor speed, \tilde{T}_E is the generator torque and \tilde{J}_r is the rotor inertia, both expressed at the low-speed shaft side, T_A is the aerodynamic torque, and P_A is the aerodynamic power expressed as (42).

$$P_A = \frac{1}{2} \rho A C_p(\lambda, \beta) v_{rel}^3 \quad (42)$$

where ρ is the air density, A is the disk surface covered by the rotating blades, v_{rel} is the relative wind speed caught by the blade and C_p is the power coefficient, which is a function of the tip speed ratio λ and the blade pitch angle β .

The blade actuator dynamic has been included in the Betti model and can be expressed as

$$\dot{\beta} = -\frac{\beta}{\tau} + \frac{\beta^*}{\tau} \quad (43)$$

where τ is the time constant of the actuator, β^* is the new control input.

Based on (37), (41) and (43), the nonlinear state-space model for the controller design is expressed as

$$\begin{bmatrix} \dot{x}_1 \\ \dot{x}_2 \\ \dot{x}_3 \end{bmatrix} = \underbrace{\begin{bmatrix} \mathbf{E}^{-1} \mathbf{F} \\ \frac{1}{2\tilde{J}_r\omega_r} \rho A C_p(\lambda, \beta) v_{rel}^3 - \frac{\tilde{T}_E}{\tilde{J}_r} \\ -\frac{\beta}{\tau} \end{bmatrix}}_{a(x)} + \underbrace{\begin{bmatrix} 0 \\ 0 \\ \frac{1}{\tau} \end{bmatrix}}_{b(x)} \beta^* \quad (44)$$

where $x_2 = \omega_r$ and $x_3 = \beta$.

A compact form of (44) can be expressed as

$$\begin{aligned} \dot{x} &= a(x) + b(x)u \\ y &= \sigma(x, t) \end{aligned} \quad (45)$$

where $x = [x_1, x_2, x_3]$, $u = \beta^*$, a and b are smooth, differentiable and known functions. y is the system output and u the control input.

4.2. Problem Formulation

When the relative wind speed allows the rotor speed to rotate at its nominal value, instabilities may occur, known as negative damping oscillations; see (3–11) of [3]. The physical explanation of this phenomenon can be explained as follows: in region 3, if the floating wind turbine pitches forward, the relative wind caught by the blades increases. This means that the aerodynamic forces and consequently the rotor speed increase. Classical controls would increase the blade pitch angle to reduce the rotor speed, but at the same time, it decreases the aerodynamic forces applied on the FOWT. This leads to letting the FOWT pitches further forward. The negative damping effect emphasizes the main challenge in controlling FOWT with two antagonist control objectives: regulation of the rotor speed to the nominal value and attenuation of the platform pitch angle.

The rotor speed tracking error e_1 can be defined as the difference between the measured rotor speed ω_r and its reference value ω_{r0} :

$$e_1 = \omega_r - \omega_{r0} \quad (46)$$

The platform pitch velocity tracking error e_2 can be defined as the difference between the platform pitch velocity $\dot{\alpha}$ and its reference value $\dot{\alpha}_0$

$$e_2 = \dot{\alpha} - \dot{\alpha}_0 \quad (47)$$

The control objective is to let e_1 and e_2 converge to the origin in finite time in the presence of the lumped disturbances.

Remark 1. To track the maximum electrical output power P_0 , the generator power tracking error can be expressed as

$$e_3 = P - P_0 = \eta_G T_E \omega_r - \eta_G T_{E0} \omega_{r0} \quad (48)$$

The generator torque has been defined constant, thus e_3 can be written as

$$e_3 = \eta_G T_E (\omega_r - \omega_{r0}) = \eta_G T_E e_1 \quad (49)$$

It is trivial that the convergence of e_1 implies the convergence of e_3 .

4.3. Sliding Variable Selection

The sliding variable is defined as

$$\sigma = \omega_r - \omega_r^* \quad (50)$$

It is assumed that all the states are available for measurement. The sliding variable is inspired by the work of [44,45] to counteract the negative damping effect. Accepting small oscillations on the rotor speed allows the attenuation platform pitch angle. Therefore, the reference rotor speed is defined as:

$$\omega_r^* = \omega_{r0}(1 + k(\dot{\alpha} - \dot{\alpha}_0)), \quad k < 0 \quad (51)$$

Replacing (46), (47) and (51) into (50), σ can be written as

$$\sigma = e_1 + c e_2; \quad c = -k \omega_{r0} \quad (52)$$

The second time derivative of σ can be expressed as

$$\ddot{\sigma} = \ddot{e}_1 + c \ddot{e}_2 \quad (53)$$

Finally, a compact form of $\ddot{\sigma}$ is given as

$$\ddot{\sigma} = f(\cdot) + g(\cdot)u + d(\cdot) \quad (54)$$

where d represents the unknown disturbances, f and g are known functions from the modified Betti model and they respect the following assumptions:

Assumption 1. $f(\cdot)$ and $g(\cdot)$ are known and bounded functions. There exist positive constant values C , K_m and K_M such as for any $x \in X$,

$$|f(\cdot)| \leq C \quad (55)$$

$$0 < K_m < |g(\cdot)| < K_M, \quad (56)$$

Remark 2. The total lumped disturbance d is Lipschitz

$$|\dot{d}| \leq D \quad (57)$$

The relative degree of the sliding variable σ is equal to two, i.e., the control input u appears in the second time derivative, as shown in (54). Thus, the so-called second-order twisting algorithm is designed in order to steer σ and its first time derivative $\dot{\sigma}$ to the vicinity of zero in finite time.

$$u = u_n + u_{SMC} = -\frac{f(\cdot)}{g(\cdot)} + u_{SMC} \quad (58)$$

where $g(\cdot)$ is invertible and u_n is the nominal control term [46]. From the undisturbed system equation of (54), i.e., $d(\cdot) = 0$, the nominal control is computed by solving u in the algebraic equation $\ddot{\sigma} = 0$ in (53).

Assuming that σ and $\dot{\sigma}$ are available, the twisting algorithm is as follows,

$$u_{SMC} = -k_1(\text{sign}(\sigma) + k_2\text{sign}(\dot{\sigma})) \quad (59)$$

Theorem 1 ([47]). Considering the sliding variable in (50) and the control input in (59), if k_1 and k_2 are selected such as

$$\begin{cases} k_1 > k_2 > 0 \\ K_m(k_1 + k_2) - C > K_M(k_1 - k_2) + C \\ K_m(k_1 - k_2) > C \end{cases} \quad (60)$$

σ converges to 0 in finite time.

4.4. Simulation Results

The simulations are performed on OpenFAST with the MATLAB/Simulink simulation tool with a sampling period of 12.5 ms. The 5 MW TLP-based FOWT is chosen among the preconfigured models in OpenFAST. The wind profile in Figure 8 is generated with TurbSim tools from the NREL [42] with a mean speed of 18 m/s based on the power law wind profile and the Kaimal turbulence model of 15% for 600 s. The wave profile is computed online by the HydroDyn module of OpenFAST with irregular waves configured from [48] with 3.5 m of the wave height and a spectral peak period of 9.08 s. This scenario has been chosen to simulate a turbulent wind speed that covers all of region 3 with relatively high wave elevations during one simulation. All the parameters of the proposed model-based twisting controller are listed in Table 3.

Table 3. Parameters of the proposed model-based twisting controller.

Control Variables	Values	Units
c	0.4537	(-)
k_1	70	(-)
k_2	35	(-)
ω_{r0}	12.1	rpm
$\dot{\alpha}_0$	0	deg

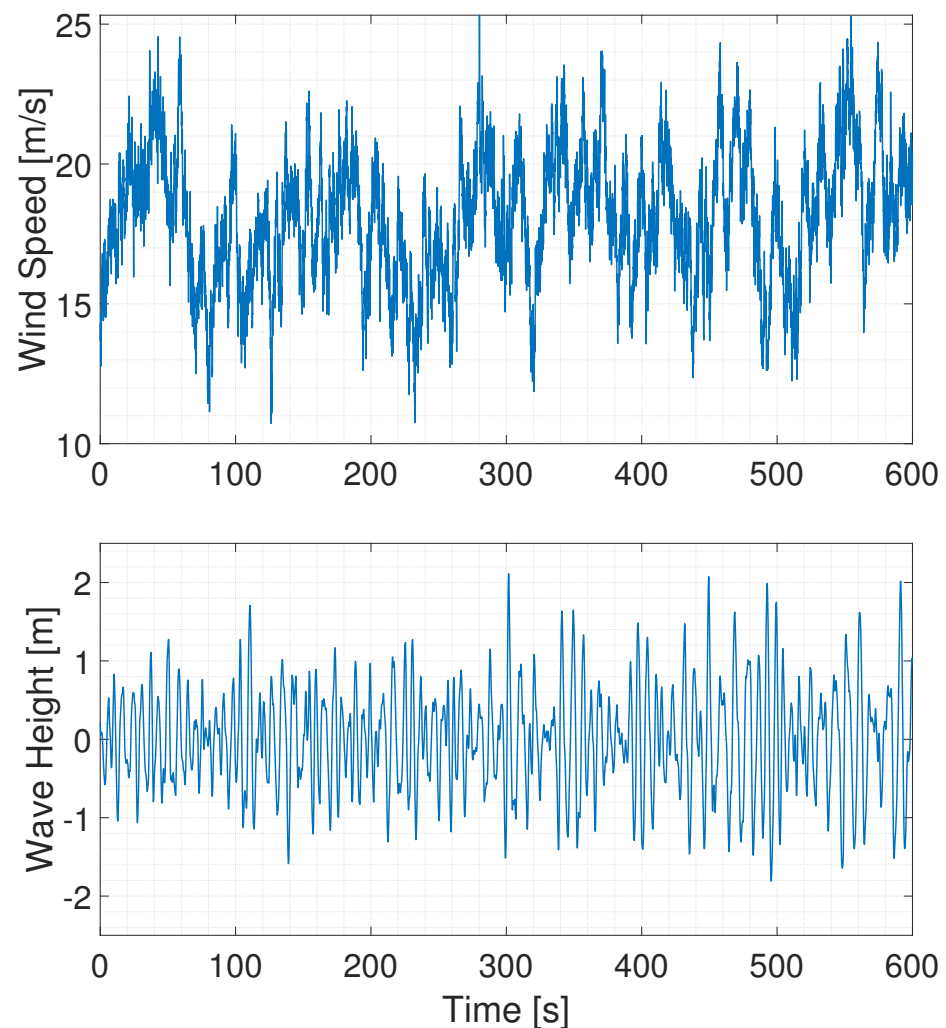


Figure 8. High turbulent wind profile (**top**) and wave height profile (**bottom**).

Combined with Table 4, Figure 9 shows the simulation results for the designed model-based twisting algorithm. The measured rotor speed is not well regulated at the exact value of the nominal rotor speed. However, it produces a mean rotor speed of around 10.57 rpm, with an STD of 1 rpm, which is quite smaller than its reference value of 12.10 rpm. As explained in [49], the generated power follows the same conclusion as the rotor speed with a mean generated power under the rated power of 5 MW and small oscillations around it.

For the platform pitch angle and the platform rate pitch angle, they are both very close to 0 degrees with a mean value of 0.0854 deg and 3×10^{-5} deg/s, respectively. The STD values show great performances of the model-based twisting algorithm with 0.2506 deg for the platform pitch and 0.3102 deg/s for the rate pitch angle. The flapwise deflection of the blade relative to its undeflected position shows large but acceptable values. This is mainly due to the behavior of the sliding mode controller that uses the total available pitch actuator capacity. This deduction can also be observed with a high amplitude of the blade command with an STD of 6.83 deg around its mean value. It can be concluded that the model-based twisting algorithm answers the control objectives in Region 3 for the 5 MW TLP-based FOWT.

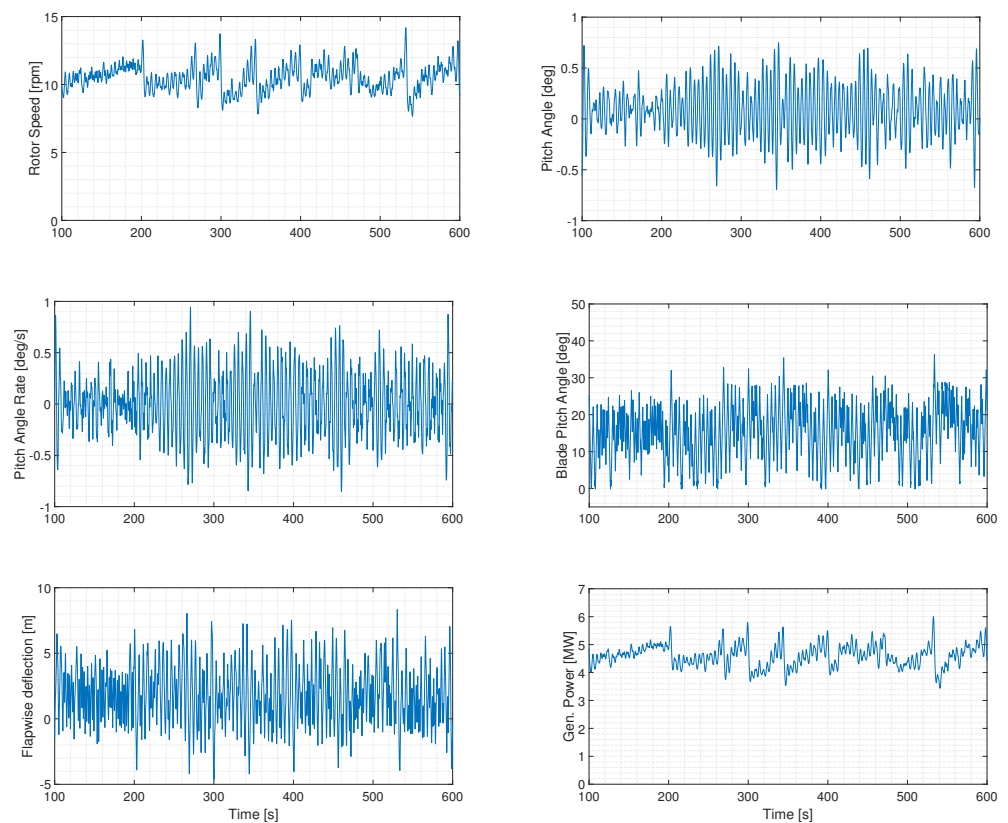


Figure 9. Simulation results of the proposed model-based twisting controller.

Table 4. Mean error and standard deviation results.

Mean ω_r (rpm)	STD ω_r (rpm)	Mean α (deg)	STD α (deg)	Mean $\dot{\alpha}$ (deg/s)	STD $\dot{\alpha}$ (deg/s)	STD β (deg)
10.57	1.02	0.0854	0.2506	3×10^{-5}	0.3102	6.83

5. Conclusions

In this article, a review of the modeling of the multi-physic floating offshore wind turbine system is proposed with considerations of the aerodynamic, hydrodynamic and mooring line models. It has been shown that the aerodynamic modules can be modeled in different manners depending on the required complexity. Similar to the classical onshore wind turbine, the novelty of this module for a floating offshore wind turbine consists in the integration of the platform pitch velocity in the expression of the relative wind speed caught by the blade. The hydrodynamic model must consider the two famous hydrodynamic modeling approaches: the linear potential flow theory with the time domain Cummins equation and the viscous theory with the Morison equation. Finally, the mooring line models can be modeled in three manners: in static, quasi-static and dynamic, thanks to external open-source code. It has been shown in this review that most of the floating offshore wind turbine models use the quasi-static model for its compromise between accuracy and time computation.

Then, a focus on nonlinear COMs is proposed, and three existing control-oriented models for three different types of FOWTs are briefly reviewed. They have been analyzed for each dynamic module: aerodynamics, hydrodynamics and mooring line dynamics, and then they have been compared with the high-fidelity code OpenFAST in simulations on Matlab/Simulink. The simulation results confirm the high accuracy of the semi-submersible-based wind turbine followed by the tensioned leg platform-based wind turbine model.

Finally, based on the Betti model, a model-based nonlinear second-order SMC is designed to regulate the rotor speed and the platform pitch angle to their respective references. The results show the benefits of such COMs for the nonlinear control design and validate that the methodology can be applied to other nonlinear COMs.

Author Contributions: Conceptualization H.B. and S.L.; methodology S.L., H.B. and Y.-C.L.; software H.B.; validation Y.-C.L. and S.L.; formal analysis H.B. and Y.-C.L.; writing—original draft preparation H.B.; writing—review and editing Y.-C.L., M.H., and S.L.; supervision S.L., M.H. and F.P.; project administration H.B., F.P. and M.H.; funding acquisition S.L., M.H. and F.P. All authors have read and agreed to the published version of the manuscript.

Funding: This research received no external funding.

Informed Consent Statement: Not applicable.

Data Availability Statement: Not applicable.

Conflicts of Interest: The authors declare no conflict of interest.

References

1. Komusanac, I.; Brindley, G.; Fraile, D.; Ramirez, L. *Wind Energy in Europe: 2020 Statistics and the Outlook for 2021–2025*; Wind Europe Report; WindEurope: Brussels, Belgium, 2021.
2. James, R.; Costa-Ros, M. *Floating Offshore Wind: Market and Technology Review*; The Carbon Trust: London, UK, 2015.
3. Jonkman, J. Dynamics modeling and loads analysis of an offshore floating wind turbine. *Natl. Renew. Energy Lab. NREL/TP-500* **2007**, *68*, 233.
4. Betti, G.; Farina, M.; Guagliardi, G.A.; Marzorati, A.; Scattolini, R. Development of a Control-Oriented Model of Floating Wind Turbines. *IEEE Trans. Control Syst. Technol.* **2014**, *22*, 69–82. [\[CrossRef\]](#)
5. Lemmer, F. *Low-Order Modeling, Controller Design and Optimization of Floating Offshore Wind Turbines*; University of Stuttgart: Stuttgart, Germany, 2018.
6. Lemmer, F.; Yu, W.; Luhmann, B.; Schlipf, D.; Cheng, P.W. Multibody modeling for concept-level floating offshore wind turbine design. *Multibody Syst. Dyn.* **2020**, *49*, 203–236. [\[CrossRef\]](#)
7. Matha, D.; Sandner, F.; Schlipf, D. Efficient critical design load case identification for floating offshore wind turbines with a reduced nonlinear model. *J. Phys. Conf. Ser.* **2014**, *555*, 012069. [\[CrossRef\]](#)
8. Lemmer, F. *Reduced Order Modeling of Floating Offshore Wind Turbines*; University of Stuttgart: Stuttgart, Germany, 2012.
9. Homer, J.R.; Ryoza, N. Physics-Based 3-D Control-Oriented Modeling of Floating Wind Turbines. *IEEE Trans. Control Syst. Technol.* **2018**, *26*, 14–26. [\[CrossRef\]](#)
10. Homer, J.R. Physics-Based Control-Oriented Modelling for Floating Offshore Wind Turbines. Master's Thesis, Mechanical Engineering, University of British Columbia, Vancouver, BC, Canada, 2015.
11. He, J.; Jin, X.; Xie, S.Y.; Cao, L.; Lin, Y.; Wang, N. Multi-body dynamics modeling and TMD optimization based on the improved AFSA for floating wind turbines. *Renew. Energy* **2019**, *141*, 305–321. [\[CrossRef\]](#)
12. Christiansen, S.; Knudsen, T.; Bak, T. Optimal control of a ballast-stabilized floating wind turbine. In Proceedings of the IEEE International Symposium on Computer-Aided Control System Design, Denver, CO, USA, 28–30 September 2011; pp. 1214–1219. [\[CrossRef\]](#)
13. Al-Solihat, M.K.; Nahon, M.; Behdinan, K. Dynamic Modeling and Simulation of a Spar Floating Offshore Wind Turbine with Consideration of the Rotor Speed Variations. *J. Dyn. Syst. Meas. Control. Trans. ASME* **2019**, *141*, 081014. [\[CrossRef\]](#)
14. Jonkman, J.; Butterfield, S.; Musial, W.; Scott, G. *Definition of a 5-MW Reference Wind Turbine for Offshore System Development*; National Renewable Energy Laboratory/TP: Golden, CO, USA, 2009; pp. 1–75. [\[CrossRef\]](#)
15. Jonkman, J.M. Influence of control on the pitch damping of a floating wind turbine. In Proceedings of the 46th AIAA Aerospace Sciences Meeting and Exhibit, Reno, NV, USA, 7–10 January 2008. [\[CrossRef\]](#)
16. Guo, H.; Lu, X.; Qiu, T. Research on pitch control of floating offshore wind turbines. In Proceedings of the 2012 9th International Conference on Fuzzy Systems and Knowledge Discovery, FSKD 2012, Chongqing, China, 29–31 May 2012; pp. 2966–2970. [\[CrossRef\]](#)
17. Li, F.; Zhou, L.; Li, L.; Wang, H.; Guo, H.; Liang, Y. Individual Blade Pitch Control for Floating Wind Turbines Bearing the Coupling of Aerodynamic—Hydrodynamic—Mooring Loads. In Proceedings of the 2019 22nd International Conference on Electrical Machines and Systems, ICEMS 2019, Harbin, China, 11–14 August 2019. [\[CrossRef\]](#)
18. Namik, H.; Stol, K. Performance analysis of individual blade pitch control of offshore wind turbines on two floating platforms. *Mechatronics* **2011**, *21*, 691–703. [\[CrossRef\]](#)
19. Namik, H.; Stol, K. Individual blade pitch control of a spar-buoy floating wind turbine. *IEEE Trans. Control Syst. Technol.* **2014**, *22*, 214–223. [\[CrossRef\]](#)

20. Raach, S.; Schlipf, D.; Sandner, F.; Matha, D.; Cheng, P.W. Nonlinear model predictive control of floating wind turbines with individual pitch control. In Proceedings of the American Control Conference, Portland, OR, USA, 4–6 June 2014; pp. 4434–4439. [\[CrossRef\]](#)
21. Zhao, P.; Nagamune, R. Switching LPV Control of a Floating Offshore Wind Turbine on a Semi-Submersible Platform. In Proceedings of the IEEE International Symposium on Industrial Electronics, Vancouver, BC, Canada, 12–14 June 2019; pp. 664–669. [\[CrossRef\]](#)
22. Shtessel, Y.; Edwards, C.; Fridman, L.; Levant, A. *Sliding Mode Control and Observation*; Birkhauser: New York, NY, USA, 2014; pp. 1–356. [\[CrossRef\]](#)
23. Komurcugil, H.; Biricik, S.; Bayhan, S.; Zhang, Z. Sliding mode control: Overview of its applications in power converters. *IEEE Ind. Electron. Mag.* **2020**, *21*, 40–49. [\[CrossRef\]](#)
24. Liu, Y.C.; Laghrouche, S.; N'Diaye, A.; Cirrincione, M. Hermite neural network-based second-order sliding-mode control of synchronous reluctance motor drive systems. *J. Frankl. Inst.* **2021**, *358*, 400–427. [\[CrossRef\]](#)
25. Liu, Y.C.; Laghrouche, S.; Depernet, D.; Djerdir, A.; Cirrincione, M. Disturbance-Observer-Based Complementary Sliding-Mode Speed Control for PMSM Drives: A Super-Twisting Sliding-Mode Observer-Based Approach. *IEEE J. Emerg. Sel. Top. Power Electron.* **2021**, *9*, 5416–5428. [\[CrossRef\]](#)
26. Zhou, Y.; Obeid, H.; Laghrouche, S.; Hilairret, M.; Djerdir, A. A novel second-order sliding mode control of hybrid fuel cell/super capacitors power system considering the degradation of the fuel cell. *Energy Convers. Manag.* **2021**, *229*, 113766. [\[CrossRef\]](#)
27. Laghrouche, S.; Plestan, F.; Glumineau, A. Higher order sliding mode control based on integral sliding mode. *Automatica* **2007**, *43*, 531–537. [\[CrossRef\]](#)
28. Zhang, C.; Tahoumi, E.; Gutierrez, S.; Plestan, F.; Deleon-Morales, J. Adaptive robust control of floating offshore wind turbine based on sliding mode. In Proceedings of the IEEE Conference on Decision and Control, Nice, France, 11–13 December 2019; pp. 6936–6941. [\[CrossRef\]](#)
29. Zhang, C.; Gutierrez, S.V.; Plestan, F.; De León-Morales, J. Adaptive super-twisting control of floating wind turbines with collective blade pitch control. *IFAC-PapersOnLine* **2019**, *52*, 117–122. [\[CrossRef\]](#)
30. Asmine, M.; Brochu, J.; Fortmann, J.; Gagnon, R.; Kazachkov, Y.; Langlois, C.E.; Larose, C.; Muljadi, E.; MacDowell, J.; Pourbeik, P.; et al. Model validation for wind turbine generator models. In Proceedings of the IEEE Power and Energy Society General Meeting, Detroit, MI, USA, 24–29 July 2011. [\[CrossRef\]](#)
31. Cline, D. *Variational Principles in Classical Mechanics*, 2nd ed.; River Campus Libraries: Rochester, NY, USA, 2018.
32. Baruh, H. *Applied Dynamics*; Springer: Cham, Switzerland, 2014; pp. 1–839. [\[CrossRef\]](#)
33. Hall, M. *AeroDyn v15 User's Guide and Theory Manual*; NREL Report; NREL: Golden, CO, USA, 2015.
34. Sebastian, T.; Lackner, M. Development of a free vortex wake method code for offshore floating wind turbines. *Renew. Energy* **2012**, *46*, 269–275. [\[CrossRef\]](#)
35. Wang, T. A brief review on wind turbine aerodynamics. *Theor. Appl. Mech. Lett.* **2012**, *2*, 062001. [\[CrossRef\]](#)
36. Namik, H.; Stol, K.; Jonkman, J. State-space control of tower motion for deepwater floating offshore wind turbines. In Proceedings of the 46th AIAA Aerospace Sciences Meeting and Exhibit, Reno, NV, USA, 7–10 January 2008. [\[CrossRef\]](#)
37. Babarit, A.; Delhommeau, G. Theoretical and numerical aspects of the open source BEM solver NEMOH. In Proceedings of the 11th European Wave and Tidal Energy Conference (EWTEC2015), Nantes, France, 6–11 September 2015.
38. Sarpkaya, T.; Isaacson, M. *Mechanics of Wave Forces on Offshore Structures*; Van Nostrand Reinhold: New York, NY, USA, 1981.
39. Masciola, M. *Instructional and Theory Guide to the Mooring Analysis Program*; Technical Report; National Renewable Energy Laboratory: Golden, CO, USA, 2014.
40. Hall, M. *MoorDyn User's Guide*; Department of Mechanical Engineering, University of Maine: Orono, ME, USA, 2015.
41. López-Queija, J.; Robles, E.; Llorente, J.I.; Touzon, I.; López-Mendia, J. A Simplified Modeling Approach of Floating Offshore Wind Turbines for Dynamic Simulations. *Energies* **2022**, *15*, 2228. [\[CrossRef\]](#)
42. Kelley, B.J.N. *TurbSim User's Guide: Version 1.5*; NREL Report; NREL: Golden, CO, USA, 2009.
43. Rahman, M. Fundamentals concerning Stokes waves. In *WIT Transactions on Engineering Sciences*; WIT Press: Southampton, UK, 1996.
44. Lackner, M.A. Controlling platform motions and reducing blade loads for floating wind turbines. *Wind Eng.* **2009**, *33*, 541–553. [\[CrossRef\]](#)
45. Lackner, M.A. An investigation of variable power collective pitch control for load mitigation of floating offshore wind turbines. *Wind Energy* **2013**, *16*, 435–444. [\[CrossRef\]](#)
46. Utkin, V.I. *Sliding Modes in Control Optimization*; Springer: Berlin/Heidelberg, Germany, 2019; Volume 53, pp. 1689–1699.
47. Fridman, L.; Levant, A. Chapter 3 Higher Order Sliding Modes. In *Sliding Mode Control in Engineering*; Routledge: London, UK, 2002; pp. 1–52.
48. Gomez, P.; Sanchez, A.L.G.; Gonzalez, G. Deliverable 1.1: Oceanographic and Meteorological Conditions for the Design; Technical Report, LIFES50+ Project. 2015. Available online: http://lifes50plus.eu/wp-content/uploads/2015/12/GA_640741_LIFES50-D1.1.pdf (accessed on 26 June 2022).